Hidden negative linear compressibility in lithium L-tartrate†

PCCP

ARTICLE

Hidden negative linear compressibility in lithium L-tartrate

Hamish. H.-M. Yeung,[a,b,*] Rebecca Kilmurray,[c,d] Claire L. Hobday,[c] Scott C. McKellar, [c] Anthony K. Cheetham,[e] David R. Allan[f] and Stephen A. Moggach[c,*]

Received 00th January 20xx,
Accepted 00th January 20xx

DOI: 10.1039/x0xx00000x

www.rsc.org/

Development of artificial muscles, next-generation pressure sensors and precision optics relies on advances in materials with anomalous mechanical properties. Negative linear compressibility, NLC, is one such rare, counterintuitive phenomenon, in which a material expands along one axis under hydrostatic pressure. Both classical and recent NLC materials face a pay-off between the active pressure range and magnitude of NLC, and in the vast majority of cases the NLC effect decreases with pressure. By decoupling the mechanical behaviour of building units for the first time in a wine-rack framework containing two different strut types, we show that lithium L-tartrate exhibits NLC with a maximum value, K_{max} = -21 TPa^{-1}, and an overall NLC capacity, χ_{NLC} = 5.1 %, that are comparable to the most exceptional materials to date. Furthermore, the contributions from molecular strut compression and angle opening interplay to give rise to so-called "hidden" negative linear compressibility, in which NLC is absent at ambient pressure, switched on at 2 GPa and sustained up to the limit of our experiment, 5.5 GPa. Analysis of the changes in crystal structure using variable-pressure synchrotron X-ray diffraction reveals new chemical and geometrical design rules to assist the discovery of other materials with exciting hidden anomalous mechanical properties.

Introduction

Negative linear compressibility (NLC) is a rare phenomenon exhibited by certain materials, which under the application of uniform pressure expand in one direction, making them highly sought after for several emerging applications that include pressure sensors, optical telecommunications and artificial muscles.[1,2] NLC can arise when coupled to a sufficiently large positive linear compression (PLC) in another axis to give overall volume reduction, which, in the absence of any phase transition, is a thermodynamic requirement at increased pressure. Isothermal compressibility, *K*, is defined as:

$$K = -\frac{1}{l}\left(\frac{\partial l}{\partial p}\right)_T \qquad \text{(Equation 1)}$$

where *l* denotes the axis length and *p* is hydrostatic pressure.

Of considerable importance is the range of pressures, Δp, in which NLC is sustained without phase transitions or material breakdown, which determines the potential applications of a given material. In classical materials, NLC is rare but may arise from a variety of mechanisms, including ferroelasticity in TeO_2 (K_{NLC} = −5.1 TPa^{-1}, Δp = 0.9-3.25 GPa), correlated polyhedral tilts in BiB_3O_6 (K_{NLC} = −6.7 TPa^{-1}, Δp = 0-5.0 GPa) or helices in elemental Se (K_{NLC} = −2.5 TPa^{-1}, Δp = 0-5.2 GPa).[2] More recently, much larger NLC effects have been discovered in molecular framework materials, which adopt wine-rack[3–11] and honeycomb[12] networks that hinge at the metal nodes. This class of materials includes metal-organic frameworks (MOFs) and offers the attractive potential for generating anomalous mechanical properties by combining different molecular or organic struts and metal ions with specific network geometries.[13–16] The flexibility of these hybrid materials can be modified using supramolecular interactions, such as argento- and aurophilic interactions[3,5,6,9] and hydrogen bonding,[7,10,11] and metastable coordination geometries,[17] which have led to a new generation of framework materials with flexibility far exceeding classical NLC materials. For example, the low pressure phase of $Ag_3[Co(CN)_6]$[3] (K_{NLC} = −76(9) TPa^{-1}, Δp = 0-0.19 GPa) shows NLC an order of magnitude greater than classical materials, whilst NLC was also reported in the MIL-53(Al) MOF system (K_{NLC} = −28 TPa^{-1}, Δp = 0-3 GPa),[8] analogous to its "breathing" effect upon gas sorption.[18]

Wine-rack frameworks that dominate the new generation of NLC materials have to date been limited to highly symmetric structures that involve just one molecular strut type, enabling the (pseudo-)tetragonal wine-rack motif to be approximated by a rhombus with just one independent strut length and

[a] *Inorganic Chemistry Laboratory, University of Oxford, South Parks Road, Oxford, OX1 3QR, UK. *Email: Hamish.yeung@chem.ox.ac.uk*
[b] *WPI International Center for Materials Nanoarchitectonics (MANA), National Institute of Materials Science, 1-1 Namiki, Tsukuba, Ibaraki, 305-0044, Japan; International Center for Young Scientists (ICYS), National Institute of Materials Science, 1-2-1 Sengen, Tsukuba, Ibaraki, 305-0047, Japan.*
[c] [c]*EaStChem School of Chemistry and Centre for Science at Extreme Conditions, University of Edinburgh, David Brewster Road, Joseph Black Building, Edinburgh EH9 3FJ, UK. *Email: s.moggach@ed.ac.uk*
[d] *Centre for Doctoral Training in Plastic Electronics, Centre for Plastic Electronics, Imperial College London, Prince Consort Road, London, SW7 2BZ.*
[e] *Department of Materials Science and Metallurgy, University of Cambridge, 27 Charles Babbage Road, Cambridge, CB3 0FS, UK.*
[f] *Diamond Light Source Ltd., Harwell Science and Innovation Campus, Didcot, OX11 0DE, UK.*

Electronic Supplementary Information (ESI) available: crystallographic information files, detailed experimental procedures and additional graphical material. See DOI: 10.1039/x0xx00000x

angle. Geometrical considerations allowed Ogborn *et al*. to decouple the pressure response of Ag(mim) (mim = 2-methylimidazolate) into three mechanical components: the strut length and angle of the rhombus plus the length perpendicular to it.[9] In this work we extend that approach to a monoclinic unit cell for the first time, to decouple the mechanical response of lithium L-tartrate, **1**, which contains two different strut types perpendicular to the unique axis. Note that **1** is denoted **9** in reference 19. In this case, four independent mechanical components can be extracted: two struts and one angle of the monoclinic wine-rack motif, plus the length of the perpendicular unique axis. By applying our extended geometrical approach to the variable-pressure and variable-temperature crystallography of **1**, we show that the dominating effect of strut compression results in a normal mechanical response at ambient pressure, but increasing flexibility in the wine-rack angle causes an unprecedented transition to anomalous behaviour – revealing so-called "hidden" NLC – above p = 2 GPa. Moreover, the negative compressibility of **1** reaches a maximum value of K_{NLC} = -21 TPa^{-1} and gives an overall NLC capacity[2] of χ_{NLC} = 5.1 %, performance indicators that are comparable to the most exceptional NLC materials to date. Such performance is all the more remarkable because at ambient pressure the thermo- and piezomechanical response is essentially normal. It is also highly significant that **1** is synthesized using green solvothermal methods from cheap, non-toxic components,[19] setting it apart from Au^+, Ag^+ and CN^--containing materials that have previously dominated the field.

Results and Discussion

The crystal structure of **1** contains two independent Li atoms, Li1 and Li2, and two separate ligands, which we herein denote L1 and L2 (see reference 18 and Figure S1 in the ESI). The basic topology can be described as a wine-rack, in which separate chains of LiO_4 tetrahedra from Li1 and Li2 are aligned along the *b*-axis and connected by tartaric acid ligands through hydroxyl groups in the *a*- direction and carboxylate groups in the [102] direction, forming two distinct interpenetrated networks (Figure 1a). Unlike previously reported NLC materials, this connectivity results in two distinct types of wine-rack struts – shorter hydroxyl-based struts and longer carboxylate struts – for which no mechanical model has yet been developed. The wine-rack networks in **1** are also intrinsically cross-linked through the ligands: L1 bridges between Li1 chains through its hydroxyl groups and those of Li2 through its carboxylates, whilst L2 does the opposite. Crystallographically, the two networks are distinct and thus the mechanical responses of their individual chemical components differ (see later section). Geometrically, however, they are identical and conversion of the crystallographic unit cell parameters by simple geometry yields the wine-rack network parameters r_1, r_2, and θ (Figure 1b). These correspond to the struts with hydroxyl-based connectivity, the struts with carboxylate-based connectivity, and the angle between them, respectively:

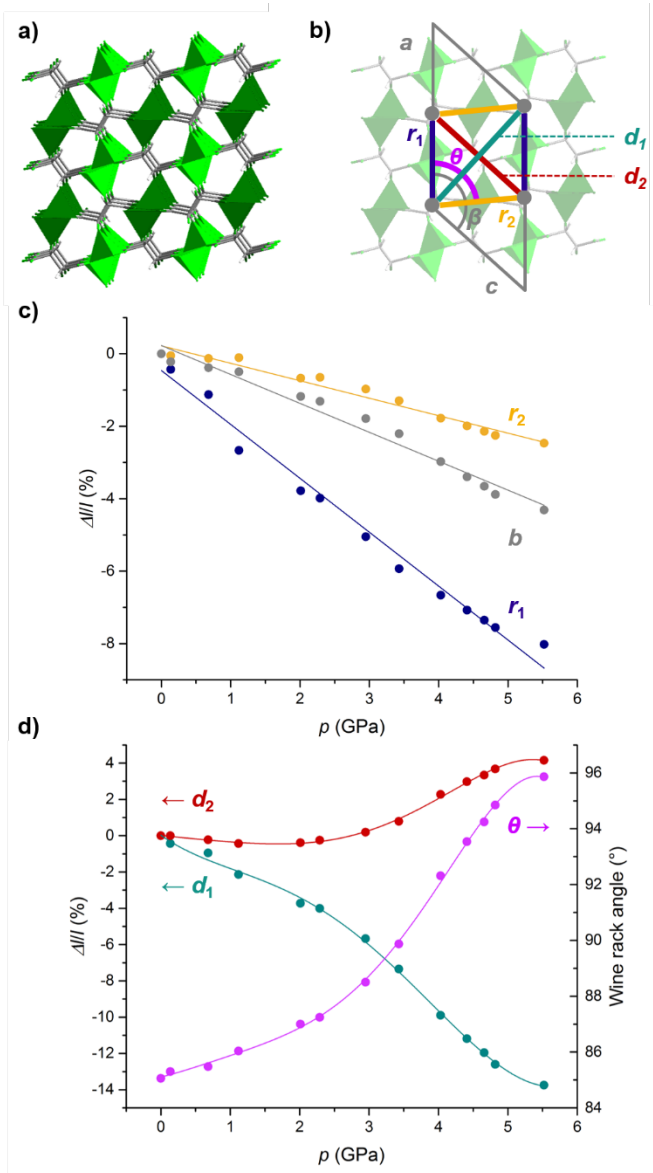

Figure 1. Structure and compressibility of **1**: a) interpenetrated networks based on Li1 and Li2 chains (dark and light green, respectively) viewed down the unique axis; b) geometrical relationship between the crystallographic unit cell (grey) and the wine-rack network parameters and diagonals (r_1, r_2, ϑ, d_1 and d_2 are shown in navy, mustard, purple, turquoise and red, respectively); c) linear changes in the lengths of wine-rack struts, r_1 and r_2, and the unit cell parameter b, with pressure; and d) changes in the wine-rack angle, θ, and diagonals, d_1 and d_2, showing polynomial fits as described in the text.

$$r_1 = {}^{a}/_{2} \qquad \text{(Equation 2)}$$

$$r_2 = \sqrt{\left({}^{a}/_{2}\right)^2 + c^2 + a.c.\cos\beta} \qquad \text{(Equation 3)}$$

$$\theta = \cos^{-1}\frac{({}^{a}/_{2})+c.\cos\beta}{r_2} \qquad \text{(Equation 4)}$$

Wine-rack structure. Figure 1c illustrates the changes in length of the wine-rack struts r_1 and r_2, and the perpendicular *b*-axis under variable pressure. All strut directions exhibit positive compressibility, with ambient pressure values of K_{r1} = 14.9(6) TPa^{-1}, K_{r2} = 4.8(3) TPa^{-1} and K_b 8.0(2) TPa^{-1} obtained from linear fits to the data according to Equation 1 (see Fig. S2).

Deconvolution of the structure of **1** into mechanical units in this way shows that, in contrast to other framework materials in which the organic struts and metal-based nodes are assumed to be incompliant,[20] **1** exhibits considerable compressibility in its struts, particularly in the direction through hydroxyl groups that cap the "inorganic" chains of LiO_4 tetrahedra, r_1. The strut dominated by carboxylate directionality, r_2, is significantly less compressible, despite the ligand's internal torsional flexibility (see later section).

Accompanying strut compression in **1** is hinging of the wine-rack at the metal nodes through the angle θ. Here it is important to point out that conventional wine-racks with rigid struts respond to pressure by closing the acute wine-rack angle, leading to volume contraction. In **1**, however, θ instead increases from 85.06° at ambient pressure to 95.86° by 5.5 GPa (Figure 1d, purple circles). It appears that this unusual expansion of θ in the low pressure region is compensated for by the strong contraction of r_1, such that the volume of **1** reduces as per thermodynamic requirements. Third-order Birch-Murnaghan fitting gives a value for the bulk modulus, B_0 = 38(2) GPa, which is in the region expected for dense MOFs, indicative of compliance somewhat intermediate between molecular materials and inorganics (see Fig S3).[13] The first derivative of the bulk modulus, B', is zero within experimental error, indicating that the material neither stiffens nor softens within the pressure range examined.

The wine-rack diagonals, d_1 and d_2, which correspond to the crystallographic [101] and [001] directions, respectively, are strongly affected by both strut compression and angle opening (Figure 1d, turquoise and red circles). Polynomial fits to the data enabled calculation of pressure-dependent compressibilities (Fig. S4, Table S1), showing that below 2.0 GPa both d_1 and d_2 exhibit normal compressive behaviour with compressibility values of K_{d1} = 26.9 TPa^{-1}, K_{d2} = 4.6 TPa^{-1} in the ambient pressure limit. The close to zero compressibility of d_2 is an effect of the competition between strut compression and acute angle opening. Above p = 2.0 GPa and at higher pressures as θ increases, the compression of d_1 is enhanced by the combination of strut compression and obtuse angle opening (Fig. 1d), reaching K_{d1} = 42.2 TPa^{-1} at p = 4.0 GPa. On the other hand, d_2 exhibits a sudden increase in length; the increase in the rate of angle opening as θ passes 90° is enough to counteract the effect of strut compression. The resulting hidden NLC effect reaches a maximum value of K_{d2} = -21.0 TPa^{-1} at p = 4.0 GPa, thereafter decreasing slightly as the rate of angle opening reduces. Similar effects, albeit with smaller magnitudes of NLC, were reported at 4 GPa in the single-strutted zinc alkyl gate compounds ZAG-4 and ZAG-6,[10] which theoretical work ascribed to proton hopping between phosphonate ligands and framework water,[11] and at 0.74 GPa in $LnFe(CN)_6$ compounds.[17] As has been found in other MOFs and molecular frameworks, the magnitude of NLC in **1** is far greater than those of canonical systems[2] but, notably, is maintained in the ambient pressure phase across a larger pressure range than most MOFs.

Principal strain axes. The compressibilities along principal strain axes were calculated from unit cell parameter changes across the whole pressure range and for the low and high pressure regions separately using the PASCal program[21] (see Fig. S5-6, Table S1). Figure 2 shows the indicatrix of compressibility below 2.0 GPa and above 2.0 GPa, overlaid on the wine-rack structure of **1**. In the low pressure region, the strong compression of r_1 causes the axis of highest compressibility to lie close to the crystallographic a-axis; the orthogonal directions have small but positive compressibility. In the high pressure region, the principal axes have rotated towards the wine-rack diagonals, d_1 and d_2, and the magnitude of PLC, along d_1, has increased. This coincides with the appearance of NLC along the c-axis, which corresponds to the wine-rack diagonal, d_2. Table 1 shows the calculated compressibilities of the principal axes, which are in good agreement with those found by polynomial fitting of the wine-rack axis lengths. Integration of pressure-dependent K_{X3} across the entire pressure range gives a value of compressibility capacity, defined by Cairns and Goodwin as the integral of compressibility with respect to pressure,[2] χ_{NLC} = 5.1 %, that is comparable to the most exceptional NLC materials to date, such as $Zn[Au(CN)_2]_2$ (K_{NLC} = −42(5) TPa^{-1}, Δp = 0-1.8 GPa, χ_{NLC} = 7.6(9) %)[12] and the high-pressure phase of $Ag_3[Co(CN)_6]$ (K_{NLC} = −5.3(3) TPa^{-1}, Δp = 0.19-7.65 GPa, χ_{NLC} = 4.0(2) %).[3]

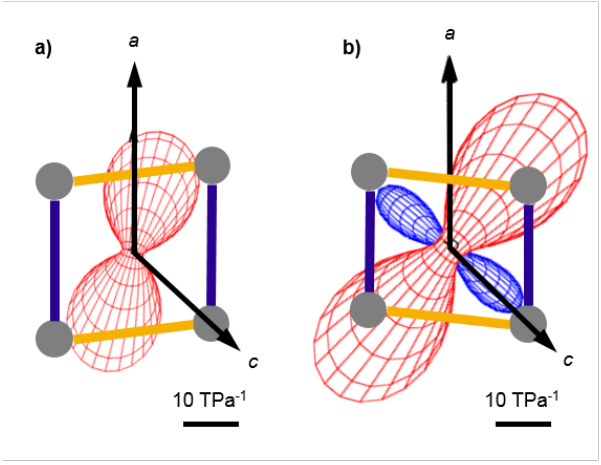

Figure 2. Compressibility indicatrices overlaid on the wine-rack structure of **1** viewed down the unique axis in the pressure regions a) 0 – 2.0 GPa, and b) 2.0 – 5.5 GPa, showing crystallographic a- and c-axes. Positive compressibility is shown in red, negative in blue.

Table 1. Compressibilities in a) the low pressure region and b) the high pressure region of **1**, comparing values and directions for the wine-rack axes and principal strain axes.

	Wine-rack axis	K / TPa^{-1}	Principal axis	K / TPa^{-1}
a)	*0 GPa limit*		*0-2.0 GPa region*	
	d_1 [101]	26.9	[0.9 0 0.4]	23(4)
	b [010]	8.0	[0 1 0]	5.6(14)
	d_2 [001]	4.6	[0.3 0 1]	-1.0(11)
b)	*4.0 GPa*		*2.0-5.5 GPa region*	
	d_1 [101]	42.2	[0.8 0 0.7]	33(3)
	b [010]	8.2	[0 1 0]	10.3(8)
	d_2 [001]	-21.0	[0.1 0 1]	-16(2)

Chemical components. Detailed examination of the coordination environments of the Li-based nodes, strut conformations and inter-ligand hydrogen bonding uncovers notable changes from ambient pressure to 5.5 GPa, which can be seen in Fig. 3. The LiO_4 environments in **1** are formed by monodentate binding of the tartrate ligands, and so the root mean squared deviation from the perfect tetrahedral geometry, δ_{tet},[22] is around 6° at ambient pressure. Upon increasing pressure, however, distortion occurs to such an extent that at 5.5 GPa δ_{tet} is above 11°, which is a similar value to the lithium tartrates that at ambient pressure feature chelation binding[19] (Fig. 3c). The bond valence sums (BVSs), which are an average measure of the shortness and strength of Li-O bonds,[23] increase by around 10 % in the region 0 GPa < p < 2.0 GPa, correlating with the compression of the structure along the a-axis (Fig. 3d). Above 2.0 GPa the BVS of Li1 continues to increase, reaching 1.37 at 5.5 GPa, whilst that of Li2 appears to plateau. This is somewhat surprising; the reason might be that it is a result of larger distortions elsewhere in the structure, which facilitate overall volume reduction. Nevertheless, the mechanical behaviour of **1** seems to be reliant on the flexibility of the closed-shell Li coordination sphere, which we previously reported could be easily manipulated by both chemical and mechanical means.[24,25] It is interesting to compare the recent findings of NLC in $LnFe(CN)_6$ compounds and Co(II) citrate, which originate directly from flexibility in the Ln(III) and Co(II) environments, respectively, rather than from any common topological mechanism.[26]

In the tartaric acid ligands, we observe large changes in torsion angles between the carboxylate oxygen atoms and the ligand carbon backbone, $\varphi_{O\text{-}C\text{-}C\text{-}C}$ (Figure 3e). Below 2.0 GPa they are largely constant at -100°, suggesting the mechanical response of **1** at close-to-ambient pressures is dominated by the Li coordination environments. Above 2.0 GPa, however, the values of $\varphi_{O\text{-}C\text{-}C\text{-}C}$ diverge from approximately -100° to -112° and -84° for ligands L1 and L2, respectively, alongside the continued distortion of the LiO_4 tetrahedra. In contrast, the carbon backbones themselves twist by less than 2° across the whole pressure range (see Fig S7). It should be noted that C-C and C-O bond distances were restrained in order to stabilize the crystal structure refinements, suppressing any reliable observation of changes in ligand bonds. However, individual covalent bonds are expected to be an order of magnitude less compressible than bond angles or torsion angles and are known to be essentially incompressible within this pressure region.[27,28]

Hydrogen bonds, which form chains of 12-membered rings along the b-axis but, individually, have significant directionality in the r_1 and r_2 directions,[19] are expected to be highly pressure-sensitive and in **1** indeed vary considerably. O-O donor-acceptor distances, $r_{D\text{-}A}$, decrease rapidly from 2.74 Å and 2.81 Å at ambient pressure for L1 and L2, respectively, to 2.64 Å in both cases at p = 5.5 GPa, indicating strengthening of the inter-ligand hydrogen bonding network (Fig. 3f).

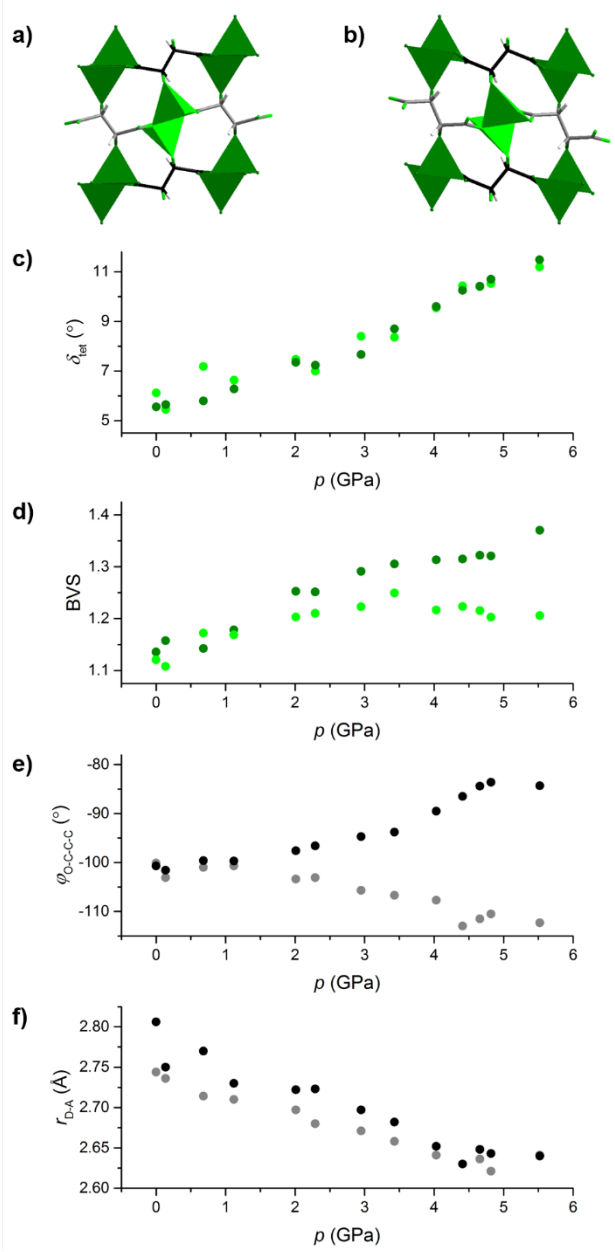

Figure 3. Changes in the chemical components of **1** with pressure: a) ambient pressure wine-rack substructure, b) 5.5 GPa wine-rack substructure, c) distortion in LiO_4 tetrahedra, δ_{tet}, d)Li-O bond valence sum, BVS, e) carboxylate torsion angle, $\varphi_{O\text{-}C\text{-}C\text{-}C}$, and f) hydrogen bonding O-O donor-acceptor distance, $r_{D\text{-}A}$. Components and data for Li1, Li2, L1 and L2 are shown in dark and light green, grey and black, respectively.

Thermomechanical behaviour. In materials with conventional wine-rack topologies, coupling between mechanical building units often gives rise to negative thermal expansion (NTE) through an "inverse relationship" of pressure and temperature, which states that structural changes upon cooling are similar to those upon compression,[29] although a counterintuitive example of a "positive relationship" was recently reported in a cationic MOF, owing to framework-guest interactions.[6] Examination of unit cell parameters using variable-temperature single crystal X-ray diffraction showed that at ambient pressure **1** instead exhibits "normal" positive thermal expansion (PTE) along each wine-rack axis (Fig. 4). Most notably, the wine-rack angle, θ, varies by just 0.2° over

the entire temperature range 120 K – 490 K (see Fig. S8), essentially rendering any hinging at the Li-based nodes negligible. Anisotropy of the thermal expansion is dictated by the underlying crystal structure: as may be expected from the relative compressibilities of each wine-rack parameter of **1** shown in Fig. 1, r_1 and d_1 are the more thermally expansive strut and diagonal, respectively.

The principal axes of PTE correlate well with those of PLC in the low pressure regime (Table S2). The magnitudes of linear thermal expansion (α_{X1} = 3.7(9) MK^{-1}, α_{X2} = 13(2) MK^{-1}, α_{X3} = 24.6(13) MK^{-1}) are small compared to common flexible MOFs,[30] suggesting that cross-linking between the interpenetrated networks acts to dampen thermal vibrations in the structure of **1**, despite the flexibility of the organic and inorganic components that is observed under high pressure.

Conclusions

By extending a geometric approach previously used for single-strutted wine-rack frameworks, we have been able to decouple the responses of the mechanical building units of more complex monoclinic frameworks that contain two different struts. Thus, we have shown that lithium L-tartrate, **1**, exhibits so-called "hidden" NLC with a large coefficient, K_{NLC} = -21.0 TPa^{-1}, and compressibility capacity, χ_{NLC} = 5.1 %, that are comparable to the most exceptional NLC materials to date. Moreover, its chemical components, lithium and L-tartrate ions, are both cheap and biologically safe compared to gold, silver and cyanide ions found in most other NLC molecular frameworks.[3,5,12] Owing to considerable strut compression, the onset of NLC in **1** is delayed to around 2.0 GPa, whilst at ambient pressure **1** exhibits normal thermal expansion, somewhat contrary to the empirical "inverse relationship" of NLC and NTE followed by most materials with the wine-rack topology.[29]

In our case, we suggest that **1** has three important characteristics that control its thermo- and piezo-mechanical response. Firstly, we observe that cross-linking of the densely-packed, interpenetrated wine-rack networks provides robustness at high pressure and also limits the magnitude of thermal expansion compared to other MOFs. Secondly, the delay in NLC response is caused by rapid strut compression – in this case, *via* distortion of the Li coordination environment – that facilitates overall volume compression and "normal" PLC mechanics at ambient pressure. This contrasts with conventional NLC materials, in which the struts are assumed to be rigid and the NLC effect is greatest in the ambient pressure limit. Normal thermal expansion in **1** at ambient pressure is simply a result of being in the regime of positive linear compressibility, which hides the NLC effect at higher pressure. Finally, opening of the wine-rack from an initially acute angle through 90°, assisted by flexibility of the inorganic LiO_4 chains and organic tartrate units, eventually overcomes strut compression to generate a large NLC effect in the wine-rack diagonals above 2.0 GPa.

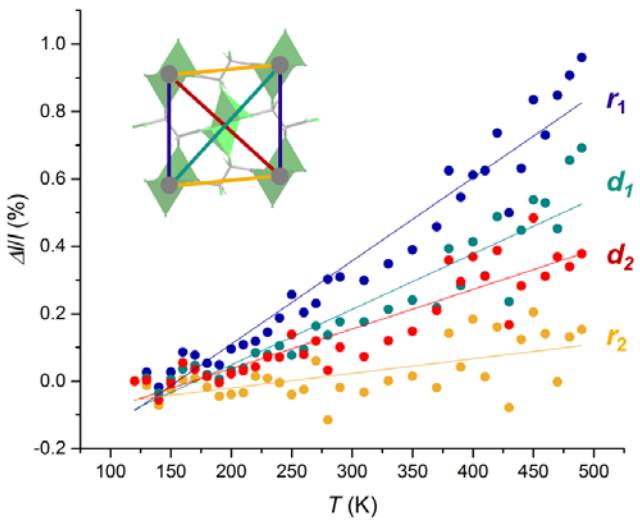

Figure 4. Variable temperature PTE behaviour of the struts and diagonals in **1**. Inset shows a schematic of the wine-rack network overlaid on the ambient pressure, ambient temperature crystal structure (colours correspond to those used in Fig.1).

Our observation of "hidden" NLC is the strongest such effect to date (although not the first[10,11,17]) and our geometric analysis of the monoclinic wine-rack structure offers a new rationale for the mechanism behind this exceptional behaviour. Furthermore, it opens up the possibility of rigorous analysis of more complex framework materials and the design of new materials in which the onset pressure and magnitude of NLC might be tuned by chemical means. Importantly, it suggests that materials previously predicted to have "normal" piezo-mechanical responses may yet exhibit anomalous mechanics at higher pressures. An obvious application for such materials would be in non-linear actuators, switches and sensors in which the NLC response is absent under ambient conditions but is switched "on" above a certain critical pressure, in contrast with conventional NLC materials in which the mechanical response is linear or decays as a function of increasing pressure. The discovery and exploitation of such non-linear NLC phases necessitates further in-situ and computational investigation, focussing on materials with the characteristics described above, in order to further understand and control stability, thermomechanical and piezomechanical response.

Acknowledgements

HHMY acknowledges support from the Glasstone Bequest for financial support through the provision of a Glasstone Fellowship and the World Premier International Research Center Initiative on Materials Nanoarchitectonics (WPI-MANA) from MEXT, Japan. CLH thanks the EPSRC and the University of Edinburgh for a studentship. SAM and SCM also thank the EPSRC for funding (EP/K033646/1). We thank Andrew Goodwin for useful discussions and Gregor Kieslich for assistance with variable-temperature single crystal X-ray diffraction. We thank Diamond Light Source for access to

beamline I19 (proposal number MT9700-1) that contributed to the results presented here.

Notes and references

‡ For experimental details of synthesis and crystallography, see Section S1, S3 and crystallographic information files in the ESI.

References:

1 R. H. Baughman, *Science*, 1998, **279**, 1522–1524.

2 A. B. Cairns and A. L. Goodwin, *Phys. Chem. Chem. Phys.*, 2015, **17**, 20449–20465.

3 A. L. Goodwin, D. A. Keen and M. G. Tucker, *Proc. Natl. Acad. Sci. U. S. A.*, 2008, **105**, 18708–13.

4 A. L. Goodwin, M. Calleja, M. J. Conterio, M. T. Dove, J. S. O. Evans, D. A. Keen, L. Peters and M. G. Tucker, *Science*, 2008, **319**, 794–797.

5 A. B. Cairns, A. L. Thompson, M. G. Tucker, J. Haines and A. L. Goodwin, *J. Am. Chem. Soc.*, 2012, **134**, 4454–4456.

6 W. Cai and A. Katrusiak, *Nat. Commun.*, 2014, **5**, 4337.

7 W. Li, M. R. Probert, M. Kosa, T. D. Bennett, A. Thirumurugan, R. P. Burwood, M. Parinello, J. A. K. Howard and A. K. Cheetham, *J. Am. Chem. Soc.*, 2012, **134**, 11940–11943.

8 P. Serra-Crespo, A. Dikhtiarenko, E. Stavitski, J. Juan-Alcañiz, F. Kapteijn, F.-X. Coudert and J. Gascon, *CrystEngComm*, 2014, **17**.

9 J. M. Ogborn, I. E. Collings, S. A. Moggach, A. L. Thompson and A. L. Goodwin, *Chem. Sci.*, 2012, **3**, 3011.

10 K. J. Gagnon, C. M. Beavers and A. Clearfield, *J. Am. Chem. Soc.*, 2013, **135**, 1252–1255.

11 A. U. Ortiz, A. Boutin, K. J. Gagnon, A. Clearfield and F. X. Coudert, *J. Am. Chem. Soc.*, 2014, **136**, 11540–11545.

12 A. B. Cairns, J. Catafesta, C. Levelut, J. Rouquette, A. van der Lee, L. Peters, A. L. Thompson, V. Dmitriev, J. Haines and A. L. Goodwin, *Nat. Mater.*, 2013, **12**, 212–6.

13 J. C. Tan and A. K. Cheetham, *Chem. Soc. Rev.*, 2011, **40**, 1059–80.

14 I. E. Collings, M. G. Tucker, D. A. Keen and A. L. Goodwin, *CrystEngComm*, 2014, **16**, 3498.

15 S. Henke, A. Schneemann and R. A. Fischer, *Adv. Funct. Mater.*, 2013, **23**, 5990–5996.

16 S. Henke, W. Li and A. K. Cheetham, *Chem. Sci.*, 2014, **5**, 2392.

17 S. G. Duyker, V. K. Peterson, G. J. Kearley, A. J. Studer and C. J. Kepert, *Nat. Chem.*, 2016, **8**, 270–275.

18 F. Millange, N. Guillou, R. I. Walton, J.-M. Grenèche, I. Margiolaki and G. Férey, *Chem. Commun.*, 2008, 4732–4.

19 H. H.-M. Yeung, M. Kosa, M. Parrinello and A. K. Cheetham, *Cryst. Growth Des.*, 2013, **13**, 3705–3715.

20 J. C. Tan, C. A. Merrill, J. B. Orton and A. K. Cheetham, *Acta Mater.*, 2009, **57**, 3481–3496.

21 M. J. Cliffe and A. L. Goodwin, *J. Appl. Crystallogr.*, 2012, **45**, 1321–1329.

22 M. M. Harding, *Acta Crystallogr. Sect. D Biol. Crystallogr.*, 2000, **56**, 857–867.

23 N. E. Brese and M. O'Keeffe, *Acta Crystallogr. Sect. B Struct. Sci.*, 1991, **47**, 192–197.

24 H. H.-M. Yeung, W. Li, P. J. Saines, T. K. J. Köster, C. P. Grey and A. K. Cheetham, *Angew. Chemie Int. Ed.*, 2013, **52**, 5544–7.

25 S. Tominaka, H. H.-M. Yeung, S. Henke and A. K. Cheetham, *CrystEngComm*, 2016, **18**, 398–406.

26 J. Binns, K. V. Kamenev, K. E. R. Marriott, G. J. McIntyre, S. A. Moggach, M. Murrie and S. Parsons, *Chem. Commun.*, 2016, **52**, 7486–7489.

27 S. A. Moggach, S. Parsons and P. A. Wood, *Crystallogr. Rev.*, 2008, **14**, 143–183.

28 J. A. Barredo-Argüeso, L. Nataf, Y. Rodrìguez-Lazcano, F. Aguado, J. González, R. Valiente, F. Rodrìguez, H. Wilhelm and A. P. Jephcoat, *Inorg. Chem.*, 2014, **53**, 10708–10715.

29 R. M. Hazen and L. W. Finger, *Comparative Crystal Chemistry: Temperature, Pressure, Composition and the Variation of Crystal Structure*, John Wiley & Sons, 1982.

30 A. U. Ortiz, A. Boutin, A. H. Fuchs and F.-X. Coudert, *Phys. Rev. Lett.*, 2012, **109**, 195502.